

Journal of Materials Chemistry A

Accepted Manuscript



This is an *Accepted Manuscript*, which has been through the Royal Society of Chemistry peer review process and has been accepted for publication.

Accepted Manuscripts are published online shortly after acceptance, before technical editing, formatting and proof reading. Using this free service, authors can make their results available to the community, in citable form, before we publish the edited article. We will replace this *Accepted Manuscript* with the edited and formatted *Advance Article* as soon as it is available.

You can find more information about *Accepted Manuscripts* in the [Information for Authors](#).

Please note that technical editing may introduce minor changes to the text and/or graphics, which may alter content. The journal's standard [Terms & Conditions](#) and the [Ethical guidelines](#) still apply. In no event shall the Royal Society of Chemistry be held responsible for any errors or omissions in this *Accepted Manuscript* or any consequences arising from the use of any information it contains.

Toughened Epoxy Polymers via Rearrangement of Network Topology

Cite this: DOI: 10.1039/x0xx00000x

M. Sharifi,^a C. W. Jang,^a C. F. Abrams,^a G. R. Palmese^a

Received 00th January 2012,

Accepted 00th January 2012

DOI: 10.1039/x0xx00000x

www.rsc.org/

The highly crosslinked molecular architecture of thermosets make this class of materials strong but brittle. It is advantageous to enhance ductility without sacrificing strength, glass transition temperature (T_g), and modulus. The hypothesis was tested that without altering chemical structure, network topology of a dense thermoset can be engineered to dissipate more energy before rupturing covalent bonds, producing a tougher material without sacrificing ultimate tensile strength, density, or glass transition temperature. A processing technique termed “Reactive Encapsulation of Solvent/Drying” (RESD) was used in which epoxy curing was conducted in the presence of varying amounts of inert small-molecule solvent, followed by a drying/annealing process in which solvent was removed. Density measurements and freeze-fracture surface analysis revealed that the resulting RESD materials are not porous in their relaxed state after annealing. Comparing the dynamic mechanical response of the modified (RESD) to the unmodified (conventional) structures revealed no significant differences in glassy modulus and T_g . However, quasi-static mechanical testing showed that upon stretching, the modified structures have volumetric energy capacity of up to 2.5 times that of the unmodified ones. SEM micrographs of fracture surfaces of RESD specimens indicated nano-sized cavities on the surface of the modified thermosets not present before breaking. Therefore, the presence of distinct topological features in the modified network is likely the origin of the large improvement in ductility. Topology-based toughening is potentially an important step toward developing better high performance network polymers and composites.

Introduction

Epoxy materials are extensively used because they typically guarantee excellent adhesion, high chemical and heat resistance, good-to-excellent mechanical properties,¹ and relatively good electrical insulating properties. Many attempts have been made to improve their resistance to abrasion when used as coating materials.² Structural epoxy-based composite materials are becoming prominent in a vast number of applications where a material with relatively high strength, high modulus and light-weight is needed. However, epoxy thermosets are brittle due to their highly crosslinked networks, and exhibit poor resistance to fracture.³⁻⁶ These polymer materials generally break before yielding without plastic deformation with relatively poor energy absorption before failure.⁷

Significant effort has been dedicated to developing methods to toughen epoxies. Toughened epoxy systems have been achieved using, for example, micro-sized liquid rubber,^{8,9} thermoplastic particles,¹⁰⁻¹³ core-shell rubber particles,¹⁴⁻¹⁵ elastomers,¹⁶ diblock copolymers,¹⁷⁻¹⁹ and interpenetrating networks.²⁰

Although these techniques were successful at toughening thermosets, it is widely observed that the presence of a soft second phase matter such as rubber particles, thermoplastic particles, or a low-stiffness interpenetrated network reduces the modulus, strength and, more importantly, glass transition temperature of the resulting system. Developing methods to toughen epoxies without sacrificing these advantageous properties remains paramount.

Recent molecular-simulation work points to a possible solution: Using coarse-grained molecular simulations of highly crosslinked polymer networks, Mukherji et al.^{8,9} observed the opening of many small random voids upon uniaxial tension, leading to a clear strain-hardening regime. These voids were not present in the unstressed samples but were encoded by the non-uniform directionality of the crosslink bonds, and these authors further showed that by tetrahedrally distributing crosslinks emanating from each particle, these voids could be suppressed, generating samples of the same density and ultimate strength as the more random samples. This work suggests that altering the network connectivity of a crosslinked polymer without changing

the crosslink density offers a route to increasing toughness without sacrificing strength.

Previous experimental work in our group offers a possible route toward realizing this suggestion. Raman et al.^{21, 22} proposed a method through which a polymer network could be tailored via a miscible and chemically inert solvent present during cure. The technique was termed Reactive Encapsulation of Solvent (RES). This method involves the synthesis an epoxy thermoset in presence of an inert solvent without microphase separation. It was shown that when the step-growth polymerization reactions take place in presence of an inert solvent that is miscible with the monomers and resulting polymer, the polymer network encapsulates the solvent species without covalent bonds being formed in the regions where inert solvent species are present. Consequently, a nanoporous polymer network is obtained upon solvent removal using supercritical extraction and drying.^{21, 22} If, as is done in this work, solvent removal is conducted simply by heating the organogels following network formation, the pores collapse leading to samples with the same density as non-RES-modified epoxies. This method of network synthesis is termed as Reactive Encapsulation of Solvent-Drying (RES-D) approach. The purpose of this article is to demonstrate how RES-D can indeed generate toughened epoxy materials without sacrificing density, strength, or glass-transition temperature, for a particular epoxy/crosslinker/solvent system. All-atom molecular dynamics simulations of the same systems further illustrate that RES-D yields inter-crosslink contour-length distributions shifted to higher values, indicating that indeed network topology is predictably influenced by RES-D.

Experimental

Materials. The materials used in this study are shown in Figure 1. The difunctional epoxy resin used is Diglycidyl Ether of Bisphenol-A (DGEBA), EPON 828 with $n=0.13$, (Miller-Stephensen Chemical Co.). The curing agent is an aliphatic tetrafunctional diamine, polyetheramine (Jeffamine D-400) with an averaged molecular weight of about 430 g/mol (Huntsman). Dichloromethane (DCM) (Sigma-Aldrich) was used as the inert solvent for the RES-D technique.

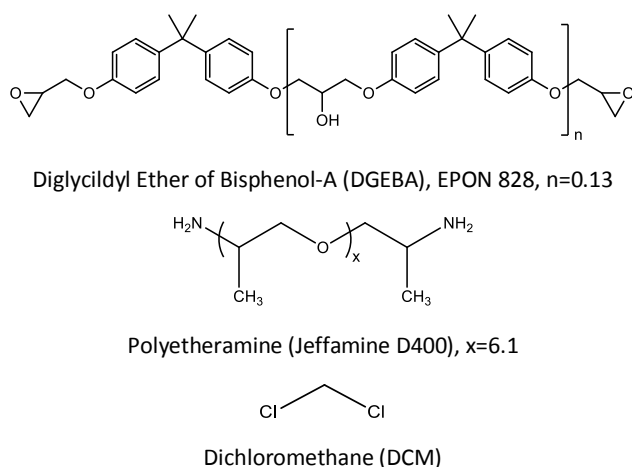


Figure 1. Molecular structures of epoxy and amine monomer resins and the solvent (DCM) used in this study.

Solvent Selection. According to Raman et al.²², the solvent used in RES has to be miscible in DGEBA and Jeffamine D400 for the entire polymerization. It also must not phase separate before or during cure. Additionally, it is essential that the solvent species remain inert during polymerization reactions and not react with any of the reactive

moieties at the curing temperature. The solvent molecules should also have a low boiling point and optimal favorable interactions with polymer chains so that they can be easily removed after polymerization but are soluble in the polymer. It is also preferred that the solvent has a low vapour pressure to minimize solvent loss during polymerization reactions at elevated temperatures. Taking into account all the above, DCM was selected as the solvent. Fourier Transform Infrared Spectroscopy in near infrared region revealed the inertness of DCM during the epoxy-amine reactions at the temperature of interest. The good miscibility observed for DCM in the reacting system likely stems from favorable weak dipole-dipole interactions involving hydroxyls formed during the ring opening reaction of DGEBA. Sample transparency (refractive indices of 1.5-1.57 and 1.42 for epoxy and DCM, respectively) before and after cure indicated the miscibility of dichloromethane during epoxy-amine reactions without macro/micro phase separation. Provided the criteria for selecting a solvent described above are met other solvents can be used to create networks of altered topology.

Resin Selection. Solvent species typically exhibit poor diffusion rate through highly crosslinked membranes.^{23, 24} Additionally, in a numerical study Rohr and Klein proposed that diffusivity of chemical species is strongly influenced by species chain lengths.^{25, 26} The preliminary experiments conducted with the epoxy resin EPON 828 and crosslinker 1,4-bis(aminocyclohexyl)methane (PACM-20). Thermogravimetric results showed that the diffusion rate of DCM through a membrane made from an aromatic epoxy resin such as DGEBA and an aliphatic amine hardener like Jeffamine D400 is about 3 to 4 times greater when compared to a system composed of same epoxy resin cured with a cycloaliphatic amine such as PACM. It is believed that the higher diffusivity of DCM in the Jeffamine-based epoxies is attributed to the greater segmental flexibility of Jeffamine (and the lower T_g). So, although polyetheramine as the curing agent provides a relatively low glass transition temperature, it was used as the curing agent in this study since it eases the solvent removal step.

Resin Processing. The sample batches were named by the weight ratio, labelled “DEA”, of DCM to the epoxy-amine resin used. For example, a “DEA 1” labelled sample has an equal weight of solvent to epoxy-amine monomers and so it is 50% solvent by weight. Batches with DEA’s of 0, 0.5, 0.75, 1, and 1.5 were prepared. EPON 828 resin was put in vacuum prior to mixing to remove water and other impurities. The purity of the EPON resin was confirmed using GPC. The value of epoxy equivalent weight, EEW, for EPON 828 was taken as 185-192 gr/eq from the material spec sheet. Jeffamine D-400 was used as received, and the amine hydrogen equivalent weight, AHEW, was assumed to be 115 gr/eq according to the material data sheet. Epoxy and amine were mixed in 2:1 molar ratio assuming ideal case where each tetrafunctional amine reacts with two difunctional epoxies. Samples were mixed in a centrifugal mixer at 2000 RPM for 10 min to ensure good mixing. The mixing process continued until a clear transparent liquid was obtained.²⁷ The samples were then poured in a perfectly sealed container to minimize loss of DCM during cure. PTFE tubes with tube vacuum couplings provided the sealed environment.

Curing Procedure. One challenge was to find the optimum curing temperature at which the polymerization approaches adequate conversion while at the same time guaranteeing the container could sustain the pressure produced by the DCM. Previous studies confirm that the rate of epoxy-amine reactions is lowered in the presence of inert solvent due to reactant dilution.²⁸ Preliminary kinetic results showed that curing reactions become extremely slow at temperatures below 50°C in the presence of DCM. DCM has a vapor pressure of approximately 2000 mmHg at 70°C,²⁹ presenting experimental challenges with sealing the curing vessel for curing temperatures

above 70 °C. We therefore were limited to a maximum curing temperature of 70 °C. All samples were kept at the reaction temperature for a total of three days to ensure the concentration of unreacted moieties is approximately zero (measured using Fourier transform infrared spectroscopy, detailed below). The same curing protocol was used for all batches including 0 DEA. All samples were weighed before and after cure to verify no solvent/resin was lost during cure. It was observed that the relative volume shrinkage after drying was larger for the specimens with higher initial solvent content.

Fourier Transform Infrared Spectroscopy (FTIR). In order to monitor the epoxy-amine reactions and to investigate the inertness of solvent molecules during epoxy-amine reactions, FTIR in the near-infrared region (4000-8000 cm^{-1}) was used. A NIR spectrometer Nexus 670/870 (Thermo Nicolet Corp.) with CaF_2 beam splitter was employed for this purpose. Capillary glass tubes (ID = 1.6 + 0.05 mm) were used to hold the samples. The tubes were sealed to ensure no solvent leakage during data acquisition. NIR spectra were collected at a resolution of 4 cm^{-1} in absorbance mode. The near infrared region was chosen since all the reactive moieties can be monitored. The peaks involved are the epoxy peak at 4530 cm^{-1} , the primary amine peak at 4925 cm^{-1} , and the primary/secondary amine peak at 6510 cm^{-1} .^{1,30}

Thermal Drying. All samples were oven-dried at 120 °C for about 20 days. The weight of each sample was recorded at regular time intervals. After 20 days, the oven was turned off and with the door closed, the samples were gradually cooled to room temperature. The time between cooling and mechanical testing was approximately the same for all samples, minimizing differences resulting from physical aging below T_g .

Dynamical Mechanical Analysis (DMA). A TA instrument Q800 DMA apparatus was utilized to measure the viscoelastic properties and T_g . All specimens were tested at a constant frequency of 1 Hz. The oscillation amplitude was kept at 15 μm in single-cantilever mode. All samples were sanded into rectangular slab geometry (35-36 mm in length, 10-12 mm in width and approximately 2 mm in thickness). Test was conducted with a scanning rate of 1 °C/min starting from room temperature to 140 °C to obtain sufficient data below and above the glass transition temperature. The T_g value was taken from the position of the peak of the loss modulus curve.

Density Measurement. The specific gravity and density of the resulting polymers was measured through the water displacement technique as described in ASTM D792. All specimens were well-polished and immersed in DI water at room temperature i.e. 23 °C. A setup as described in ASTM D792 was used to measure wet weights and density was measured using the procedures described therein.

Density values at the elevated temperatures (e.g. $T = T_g + 40$) were found by adjusting the room temperature density using volume expansion data obtained using a TA Instruments Q400 TMA apparatus.

Quasi-static mechanical properties. Uniaxial quasi-static mechanical properties in tensile and compressive modes were determined using a servohydraulic Instron apparatus model 8872. Five identical specimens were prepared for each sample type. They were cut into a rectangular slab geometry and then plastic tabs glued at each end. They were also well-polished to minimize the adverse effect of surface roughness on the resulting stress-strain curves. All dimensions were uniform with a standard deviation of $\pm 1\%$. All samples were drawn under a uniaxial tensile loading rate of 0.5 mm/min at room temperature. The compression specimens were prepared the same way where five identical cubic specimens (3x3x3 mm $\pm 2\%$) were put in order for each of the sample types.

Compressive load was applied in the axial direction at a crosshead speed of 1 mm/min at room temperature. The stress-strain data was collected until the point of rupture.

Scanning Electron Microscopy (SEM). High resolution micrographs were taken with a Zeiss Supra 50VP equipped with an in-lens imaging detector. The samples were all broken at either room temperature or in liquid nitrogen. All the fractured surfaces were platinum sputtered for 25 seconds prior to imaging. The sputtering duration is selected to avoid covering the visible features on the broken surfaces with the sputtering material.

All-atom Molecular Dynamics (MD) Simulations. The GAFF force field,^{31, 32} and the LAMMPS simulation package,³³ was used to conduct all-atom MD simulations of stoichiometric Epon/Jeffamine/DCM epoxies. Each simulation system was generated by first placing stoichiometric amounts of Epon828 and Jeffamine-D400 (J400) were followed by the desired amount dichloromethane to obtain low density mixture in a periodic box. The concentration of DCM in the mixtures was identical to those the experiments; i.e., 0%, 33%, 40%, and 50% by weight DCM. Four replicas per DCM concentration were generated. A series of NVE (constant number, volume and energy) and NPT (constant number of atoms, constant pressure, and constant temperature) simulations were initially performed on each system to achieve an equilibrium density value of about 1.07 g/cm^3 . Then, a multi-step crosslinking algorithm was applied to make three-dimensional network structures.³⁴ Polymerization involves the epoxide groups in Epon828 and the amine groups in Jeffamine D400 and results in a crosslinked network. Once a fully reacted crosslinked polymer was successfully achieved, DCM molecules were eliminated. Each system was annealed afterwards in the NPT ensemble for 5 ns at 600 K. Finally, each system was cooled with a rate of 0.2 K/ps and equilibrated for 200 ps every 50 K decrement until 300 K was reached. Dijkstra's algorithm³⁵ was used to find minimum contour path length for each unique pair of amine nitrogen atoms. More details of the simulations are given in recently published work by our groups.³⁶

Results and discussion

Curing. Figure 2 shows FTIR spectra at various time-points over two days of curing at 70 °C for a typical DCM – DGEBA/Jeffamine D400 systems (0.5 DEA). These data indicate completion of epoxy-amine reactions in the presence of dichloromethane for stoichiometric amounts of DGEBA to Jeffamine D400 as the epoxy, primary amine, and primary/secondary amine peaks at 4530 cm^{-1} , 4925 cm^{-1} and 6510 cm^{-1} all disappear following cure.

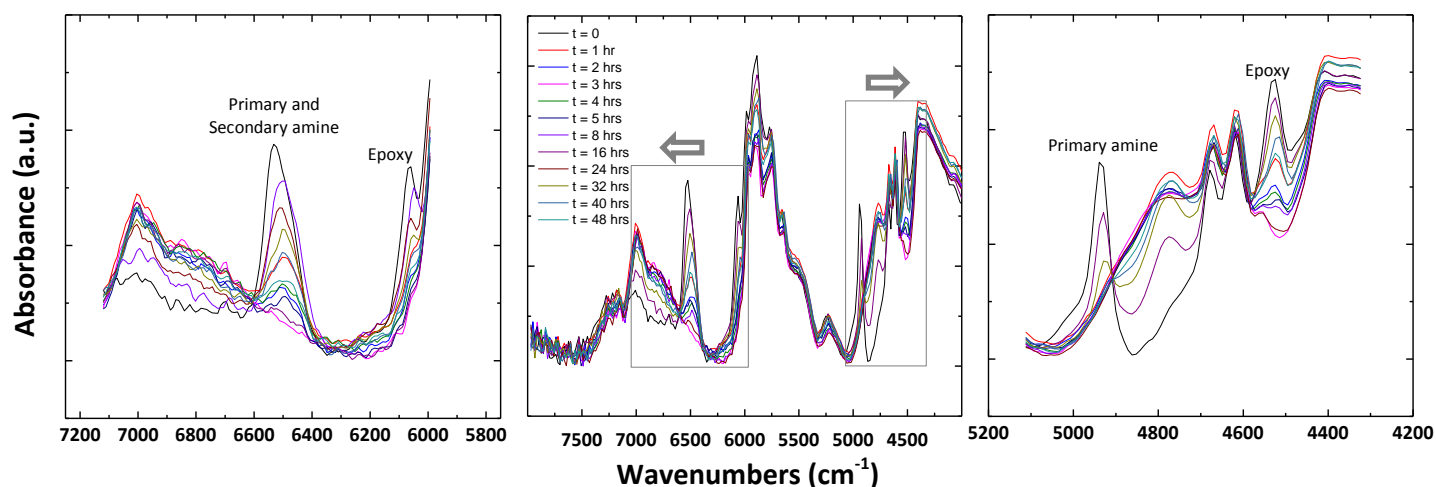


Figure 2. FT-NIR spectra for epoxy-amine reactions for a sample containing dichloromethane (0.5 DEA) at 70°C.

Drying. Thermo-gravimetric data during post-cure drying are shown in Figure 3. The plateau in weight-vs-time indicates the termination of drying. In addition, weight loss was in good agreement with the initial amount of solvent used. Nearly 99% of initial solvent was removed in all cases.

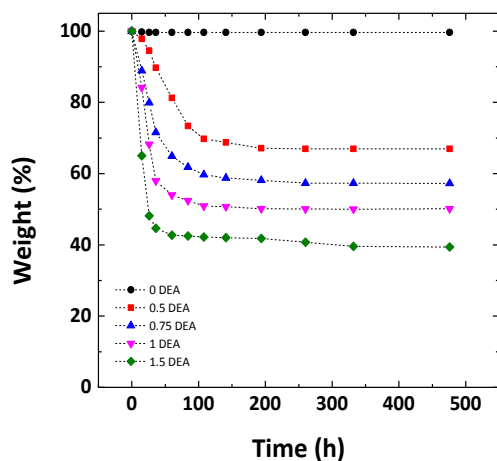


Figure 3. Thermo-gravimetric analysis at 120 °C for samples with different initial solvent amounts.

Bulk Density. The original RES method using supercritical extraction was developed to synthesize nanoporous thermosets.²⁸ In the RESD approach, drying above T_g and long-time annealing is hypothesized to fully collapse these voids, yielding samples with the same density as neat-cured epoxies. Average density values and their standard deviations for the dried specimens at room temperature, and their corresponding estimated values for $T = T_g + 40$ °C are listed in Table 1. Statistically invariant density values for all samples support the claim that the free volume fraction is comparable for unmodified and modified systems implying that the modified structures should have collapsed voids. Furthermore, equal density values at $T = T_g + 40$ °C indicate that the hypothesized void structures remain collapsed in the rubbery state.

Table 1. Averaged density values at room temperature and 40 °C above T_g .

	$\rho_{T=23^\circ\text{C}}$ (g/cm ³)	$\rho_{T=T_g+40}$ (g/cm ³)
0 DEA	1.123 ± 0.002	1.106
0.5 DEA	1.127 ± 0.012	1.109
0.75 DEA	1.129 ± 0.005	1.112
1 DEA	1.129 ± 0.009	1.111
1.5 DEA	1.126 ± 0.012	1.109

Dynamical Mechanical Properties. The hypothesis of polymer network structural differences for the resulting thermosets are investigated using dynamic mechanical analysis in this section. According to Raman et al.²⁸ nonbonded domains form throughout a polymer network during step-growth polymerization in the presence of an inert solvent, leaving pores when the solvent is removed by supercritical extraction. However, thermal drying above T_g allows the polymer chains to relax and the resulting voids to collapse. The collapsed voids, referred to as “protovoids” in this study, do not provide additional free volume (as shown in the “Bulk Density” section). The concept is illustrated schematically in Figure 4 – note that in all cases each crosslinking point has the same number of connections and that after drying the density of the modified system is the same as that of the unmodified system. Therefore the glassy modulus of the modified thermosets is expected to be comparable to the value of the unmodified thermosets. DMA results described below indicate that the glassy modulus at room temperature for modified thermosets is comparable to that of the unmodified 0 DEA resin, implying that the probable structural variations do not sacrifice the material’s glassy modulus.

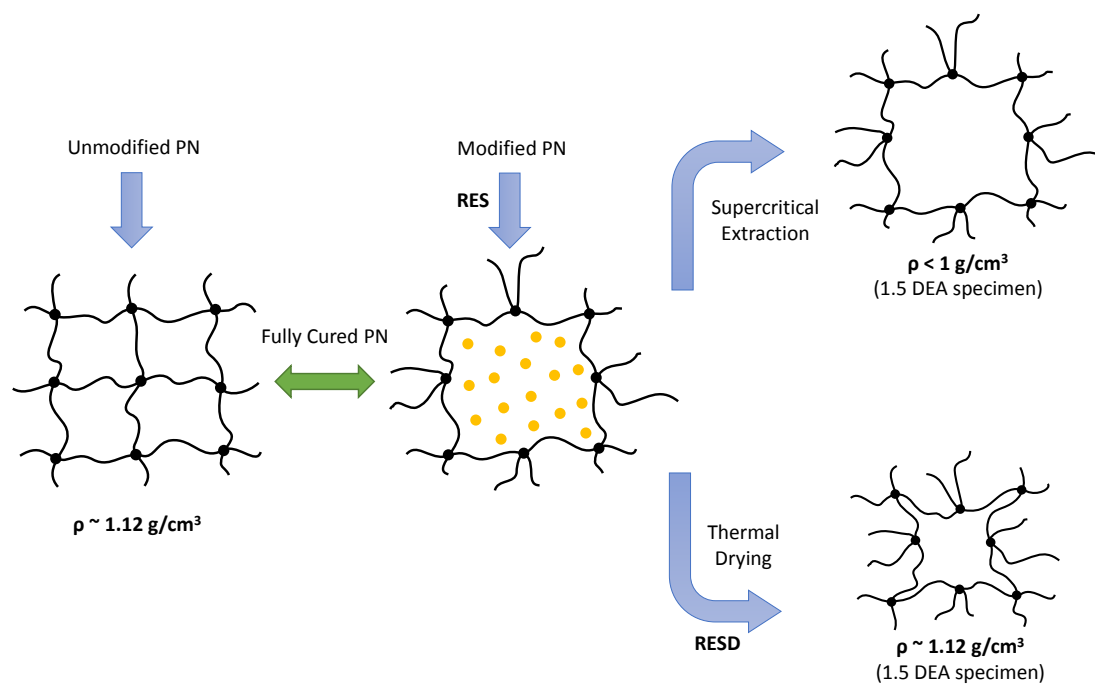


Figure 4. 2D schematic network structure of a neat-cured epoxy and modified epoxy through RES and RESD. The upper right is when solvent is removed through supercritical extraction and lower right is when solvent removed through thermal drying.

Figure 5 shows of storage and loss moduli vs. temperature for the dried specimens. Additionally, Table 2 contains a summary for all samples tested of RT glassy modulus, rubbery modulus ($T = T_g + 40$ °C), T_g obtained as the peak position of the loss modulus vs. temperature plots in Figure 5, and the height of the $\tan \delta$ peak (not shown in Figure 5). Based on the results shown in Table 2, the glass transition temperature has not been affected through the use of RESD. Considering the fact that solvent typically reduces the glass transition temperature as well as Young's modulus, invariant T_g in our samples indicate that any residual solvent in the dried samples is negligible.

Table 2. DMA results: RT glassy modulus, rubbery modulus ($T = T_g + 40$ °C), glass transition temperature, and peak values of $\tan \delta$.

	E_g (GPa)	E_r (MPa)	T_g (°C)	Tan δ peak
0 DEA	2.30	10.71	59.9 ± 0.3	1.23
0.5 DEA	2.16	7.15	57.7 ± 0.9	1.45
0.75 DEA	2.35	5.92	59.2 ± 1.3	1.4
1 DEA	2.25	5.36	59.0 ± 1.1	1.55
1.5 DEA	2.25	5.21	58.5 ± 1.0	1.56

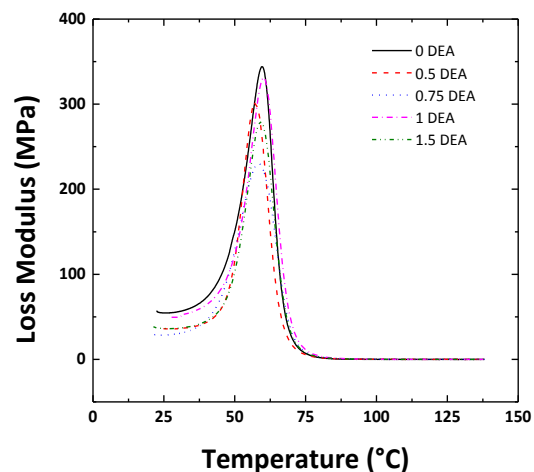
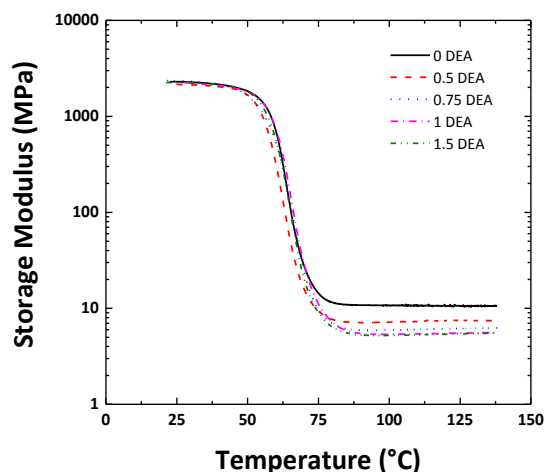


Figure 5. Dynamic Mechanical properties of the thermal heated samples with different initial solvent content. Storage Modulus vs. Temperature (left), and Loss Modulus vs. Temperature (right). The glass-transition temperature is taken as the peak position of loss modulus curves.

Although the glassy moduli and T_g values are comparable for the dried unmodified and modified samples, the differences in $\tan \delta$ peak and rubbery modulus were significant. The difference in $\tan \delta$ peak is shown in Figure 6, and the variation of rubbery modulus will be elucidated in the next section.

The results indicate that both $\tan \delta$ peak value and the area under $\tan \delta$ is greater for modified samples. The tangent of the phase angle δ , $\tan \delta$, is defined as the ratio of loss modulus over storage modulus, which is a measure of energy dissipation.⁷ It also shows the extent of internal friction or damping and so this quantity is a sensitive measure of molecular structure in a polymer network. For two homogenous thermosets where the distribution of molecular weight between crosslinkable sites is almost uniform, the one with a loosely crosslinked network typically shows a higher peak value and subsequently a larger area under $\tan \delta$ because viscous behaviour dominates over elastic behaviour, particularly above T_g .^{37,38} A highly crosslinked polymer network has a reduced chain slippage, and so a lower $\tan \delta$ peak value at elevated temperatures.³⁹ In the current study, it is shown that the peak values of $\tan \delta$ are higher for the modified samples. It implies that either the crosslinking density is lower or relative chain slippage between crosslinks is higher for the modified samples, and thus the modified thermosets can absorb more energy under cyclic stress. Since both modified and unmodified thermosets are fully cured with the same density, and therefore must have comparable crosslink densities, the observed difference in viscoelastic properties could be due to network topology differences.

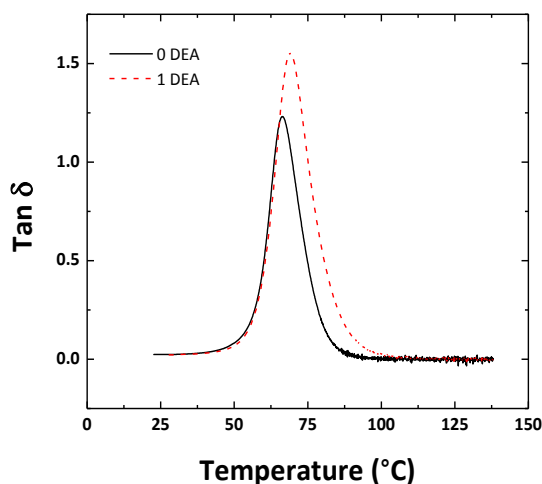


Figure 6. $\tan \delta$ vs. temperature for unmodified (0 DEA) and modified (1 DEA) samples.

Topological Differences. One important observation in this study is the decreasing trend in rubbery modulus when increasing the initial solvent-to-monomer weight ratio of the dried samples (Figure 5).

The molecular weight between crosslinks, M_c , and crosslink density, ν , for an amorphous polymer network above its glass transition temperature can be obtained using the following relations derived from rubber elasticity theory:³⁹

$$M_c = 3 \frac{\rho RT}{E} \quad (1)$$

$$\nu = \frac{\rho}{M_c} \quad (2)$$

Crosslink density (ν) and molecular weight between crosslinks (M_c), are plotted in Figure 7 as a function of initial solvent-to-monomer ratio using Equations 1 and 2 and density and rubbery modulus data obtained at $T = T_g + 40$ °C given in Tables 1 and 2 respectively.

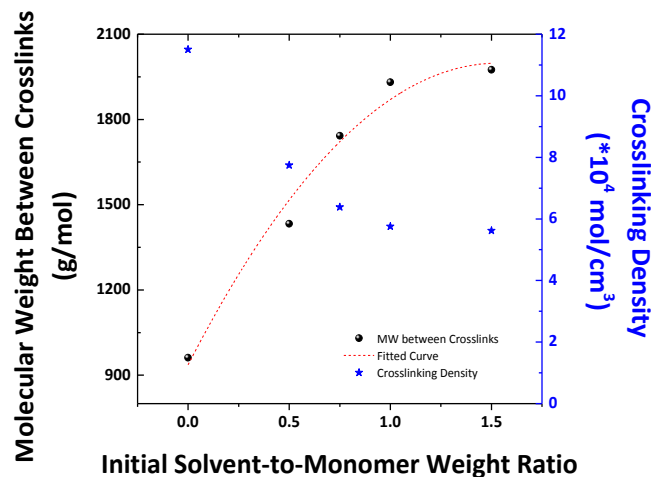


Figure 7. Apparent molecular weight between crosslinks and apparent crosslinking density vs. initial solvent-to-monomer weight ratio. Samples are fully reacted and identical in composition.

The reduced plateau rubbery modulus for modified specimens is not due to inadequate polymerization. FT-NIR spectra showed that epoxy-amine reactions are the predominant reactions for systems with or without solvent. Additionally, all show an ultimate conversion greater than 99% for epoxide reactive groups. Macosko et al.⁴⁰ related the molecular weight between crosslinkable sites to the extent of crosslink formations. According to this theoretical relationship, the extent of reaction beyond gelation for the resulting thermosets should be much lower than unity to provide identical M_c values corresponding to the ones measured for our modified samples. This difference is larger than the error attributed to the conversion levels obtained from FT-NIR and so the extent of cure is not the reason for the elevated values of molecular weight between crosslinks. Moreover, it has been discussed that glass transition temperature is a sensitive measure of extent of polymerization,⁴¹⁻⁴³ and any deviation from full cure conversion should result in a drastic decrease in the glass transition temperature. From this perspective, the comparable T_g values indicate that the reduced rubbery plateau was not caused by differences in extent of polymerization.

The topological distance between crosslinks is anticipated to be a parameter that differs substantially when comparing unmodified to modified systems. This offers an explanation for the observed differences in rubbery plateau moduli that is not predicted by theory if the crosslink density is kept constant. Topological distance is defined as the average of all distances from one crosslink point to all of the neighboring crosslinks when tracing the network, in contrast to spatial distance which is the average of all the straight distances from one crosslink point to all the neighboring crosslinks. The distinction between spatial and topological distance is shown in Figure 8. Note that for our dried systems the spatial distance between crosslinks does not vary because the number of crosslinks (composition) remains the same.

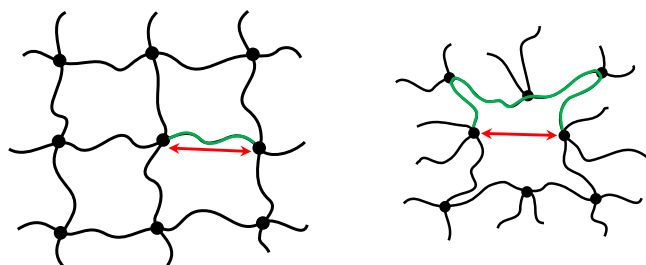


Figure 8. 2D schematic of an unmodified (left) and a modified (right) polymer network. Green lines are the topological distances, red arrows are the spatial distances and dots are crosslink points. Modified network structure has collapsed voids with identical intermolecular packing to the unmodified structure.

Considering an unmodified system, it is believed that the average topological distance from one crosslink point to all the neighboring crosslinks is comparable (although larger) to the average spatial distance. However, for a modified system, average topological distance is greater than the corresponding spatial distance. This concept is also illustrated in Figure 8. From statistical thermodynamics, the number of chain conformations and subsequently entropy will be higher for the modified systems assuming that the entropic term is governed by topological distance rather than end-to-end distance. Since retractive force and subsequently retractive stress of a polymer network in rubbery state is inversely proportional to the entropy of the system, the resulting rubbery modulus is reduced for modified systems. This could lead to observed apparent elevated molecular weight between crosslinks for the modified systems.

Swelling. Results of swelling experiments confirm that significant topological differences are introduced by curing the epoxy-amine systems in the presence of an inert solvent. Dried samples were soaked in dichloromethane at room temperature for a period of time sufficient to attain equilibrium. The observed equilibrium solvent mass uptake for the 0 DEA, 0.5 DEA, and 0.75 DEA samples was 111%, 150%, and 170% respectively. Thus equilibrium swelling increases with increasing solvent content used to prepare the samples. Since all the thermosetting systems are fully crosslinked, and chemically the same, the equilibrium mass uptake enhancement is a result of altered polymer network topology.

Minimum Topological Contour Lengths from All-Atom Simulations. So far, the hypothesis was that, presence of DCM should alter the topology of a crosslinked polymer network, since DCM molecules must restrict local directions in which crosslink bonds can form. It was also hypothesized that the topological distance is distinguishable between the two network structures. In order to investigate this question, the minimum contour path from every nitrogen atom to every other for each simulated crosslinked sample was measured using all-atom MD simulations. The average minimum inter-nitrogen contour path for each system is shown in Figure 9. Here a clear signature of the effect of including DCM during cure is observed, in that the minimum contour path distributions shift to larger path lengths as the during-cure DCM concentration increases. The effect is strongly pronounced at the largest path lengths. The results of a more detailed study by our groups have recently been published.³⁶

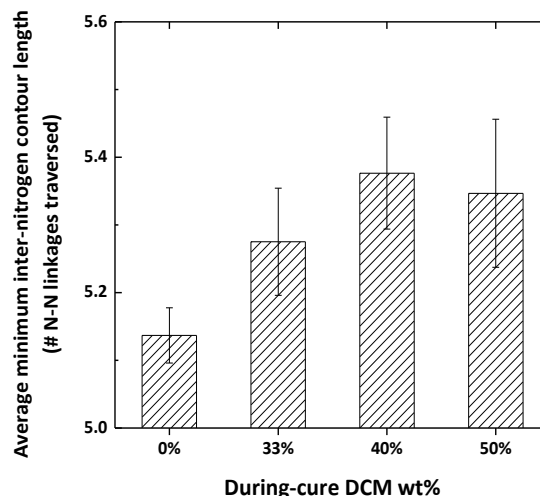


Figure 9. Average minimum inter-nitrogen contour length as function of the initial amount of DCM from all-atom MD simulations.

The trend in minimum contour length with solvent content mimics that of the $\tan \delta$ peaks and apparent molecular weight between crosslinks. Clearly the all-atom structures reflect the influence of solvent on the network topologies. This result is significant because the minimum contour path between any two points represents the largest Euclidean distance to which those points can be separated in straining the system before covalent bonds must yield. Therefore it is hypothesized that minimum contour paths between points in a network could influence large-scale material properties, such as toughness, that depend less on intermolecular packing and more on sacrificing covalent bonds. That we see twin correlations (a) between RESD solvent content and toughness and (b) between RESD solvent content and longer minimum contour paths justifies ongoing work in our labs to establish links between network topology and material properties.

Quasi-Static Tension. As shown, RESD does not sacrifice the glass transition temperature and glassy modulus of the cured thermosets. It was also discussed that the modified samples contain structural features in the form of collapsed voids. According to Mukherji et al.⁸ expansion and growth of these protovoids without bond breaking is the microscopic origin of strain hardening in a glassy polymer which yields a more ductile material. To investigate this hypothesis, mechanical response of each of the materials to uniaxial tensile and compressive loading was captured.

Uniaxial stress-strain curves for the unmodified and modified tensile coupons were recorded for at least five identical specimens for each data point. A very large plastic deformation for the modified samples was observed, as shown in Figure 10. Although necking starts for both types of specimens at strain values of around 10%, modified samples also exhibited extensive drawing. The drawing is a result of the local stress rising sufficiently during necking so that it is sufficient to stretch material at the edge of the neck increasing the size of the necked region. It is interesting to note that the behaviour exhibited by the 1.5 DEA sample in Figure 10 is similar to that observed for semicrystalline thermoplastics where the ability to sustain drawing is a result of large changes in microstructure with significant strain hardening. Note that engineering stress and strain was used in reporting these data as this is the most common way of reporting such data. Furthermore, simple conversion to real stress strain does not provide additional insight since the necking results in an inhomogeneous distribution of strains and stresses along the length of

the sample. Nevertheless it is important to realize that the stress in the necked region is significantly higher than shown by the stress-strain plots in Figure 10.

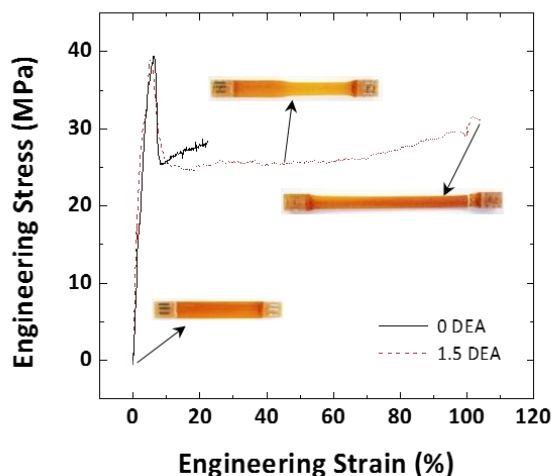


Figure 10. Engineering stress-strain curve for unmodified, 0 DEA, (solid black line) and modified, 1.5 DEA, (red dashed-line) samples in tensile mode.

It is suggested that this remarkable improvement in ductility, or toughness, is primarily due to the topological differences between unmodified and modified polymer networks as discussed. Opening of protovoids without bond breaking would enable the thermoset to plastically elongate under tensile deformations as illustrated schematically in Figure 11. Also contained in Figure 11 are SEM images of the fracture surfaces of 0 DEA (a) and 1.5 DEA (b) samples. The modified sample fracture surfaces clearly show nano scale cavities not present in the unmodified systems.

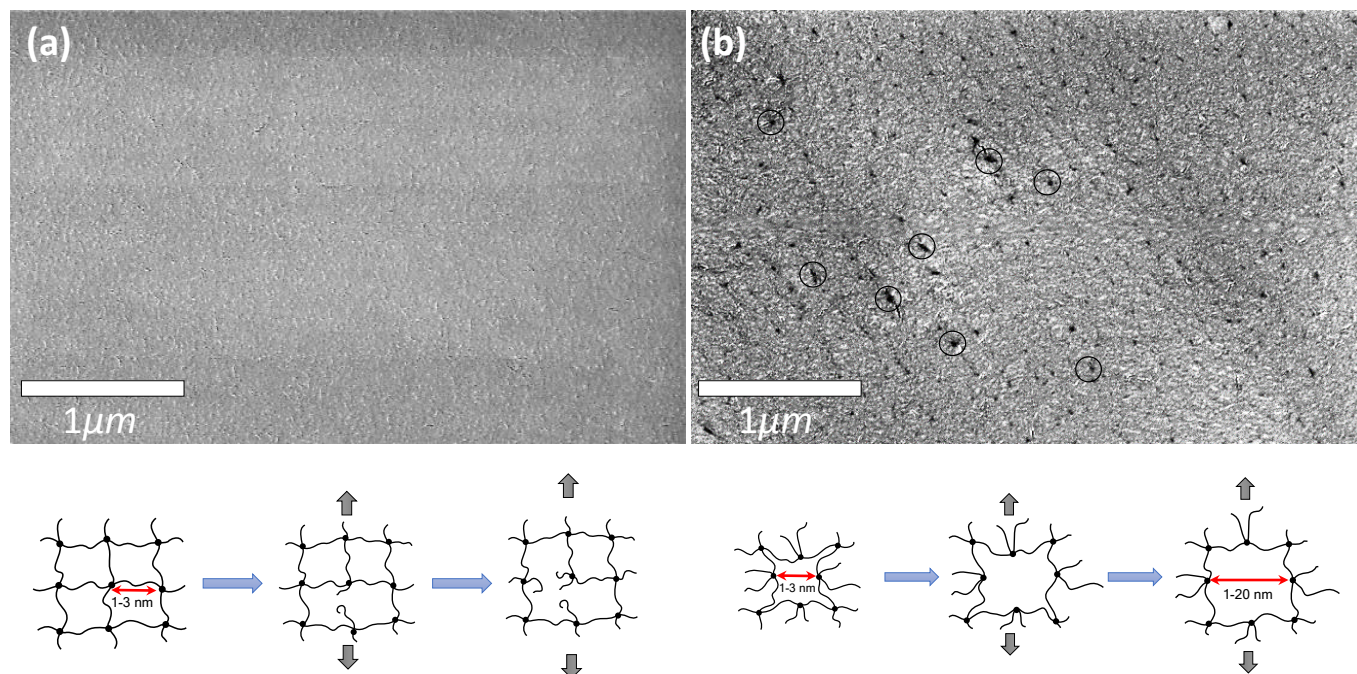


Figure 11. RT-fracture surface of unmodified (a) and modified (b) structures. Scale bars are 1 μm in size. The schematic is representative of network deformations and bond reorientations during protovoid growth under tensile stress. Some of the holes are pointed with circles in the modified (b) structures.

Evidence of stress relaxation was observed in the necked region after testing. In a separate study, drawn samples were annealed at room temperature, and above T_g ($= 60\text{ }^\circ\text{C}$). Samples annealed at room temperature deformed slightly, whereas the samples annealed above T_g recovered their original shape. The shape recovering capacity of highly elongated samples suggest that covalent bond rupture was not prevalent during tensile deformation. This suggests that the improved ductility of the modified samples arises from enhanced molecular mobility associated with the disruption of weak interactions at the interfaces of the protovoids.

Average values of toughness and failure strain are shown for each batch of samples in Figure 12. In this study, toughness refers to the total area under stress-strain curve to the point of fracture, and it is a measure of ductility. In addition, failure strain is defined as the strain value at which the sample breaks. As can be seen in Figure 12, toughness increased with initial DCM content up to a solvent-to-monomer weight ratio of 0.75, beyond which no further increase is observed. The trend of failure strain was similar to that of toughness. Generally, thermoset toughness can be increased by using more flexible crosslinkers, but more flexible crosslinkers generally means lower T_g 's.⁹ We use relatively flexible Jeffamine crosslinkers, but across our values of solvent-to-monomer initial weight ratios, T_g is essentially invariant while ductility is greatly enhanced. This demonstrates that the toughening effect due to the expansion of protovoids does not sacrifice T_g . In addition, Young's modulus (E) and tensile strength at yield (σ_y) are listed in Table 3. The results show no significant statistical differences between unmodified and modified samples, demonstrating that the enhancement in ductility is

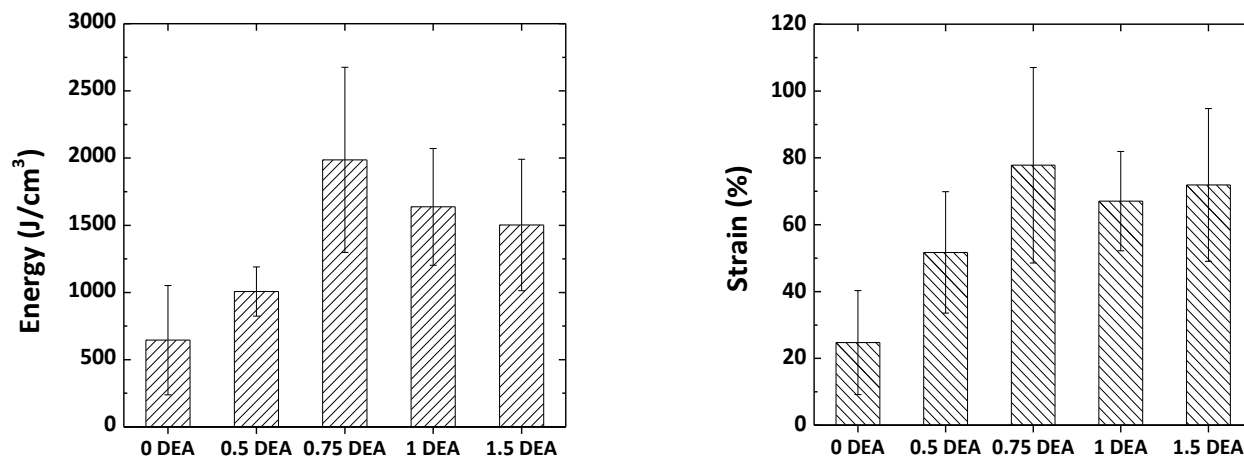


Figure 12. Average toughness (left) and failure strain (right) values for each sample under uniaxial tensile load. Error bars indicate the distribution around statistical averages.

obtained also without sacrificing Young's modulus and tensile strength.

Table 3. Tensile properties (engineering) under uniaxial tensile load at room temperature.

	E (GPa)	σ_y (MPa)
0 DEA	2.4 ± 0.2	34.6 ± 2.2
0.5 DEA	2.2 ± 0.2	32.0 ± 2.6
0.75 DEA	2.3 ± 0.1	38.9 ± 0.6
1 DEA	2.2 ± 0.1	35.7 ± 1.9
1.5 DEA	2.4 ± 0.1	31.9 ± 2.3

Void Size and Density. Raman et al.²² showed that in the RES technique using supercritical drying, average pores size of a nanoporous polymer network can be tailored through the initial solvent-to-monomer weight ratio. This suggests that the sizes of the protovoids generated using RESD would also increase with increasing solvent content and that the size might also be linked to improvement in ductility of the modified thermosets. Assuming that the features observed in the fracture surfaces of modified systems are indeed related to the size of the collapsed voids, protovoid size was investigated by quantitatively analysing SEM micrographs of such surfaces. An image processing tool, ImageJ, was utilized to determine the average pore size and surface density. Figure 13 shows estimates of void diameters for samples from each batch. The error bars associated with each mean is the standard deviation obtained from at least three images at different surface locations. We observe that the average void diameter for the relatively circular features, with circularity of 0.3-1, is roughly 20-22 nm. According to Raman et al.²², the average pores size of the nanoporous thermosetting networks obtained from 0.5 and 0.75 solvent-to-monomer weight ratios in RES was 2.4 and 3.2 nm. The features observed in our work are significantly larger perhaps because of deformation induced by loading.

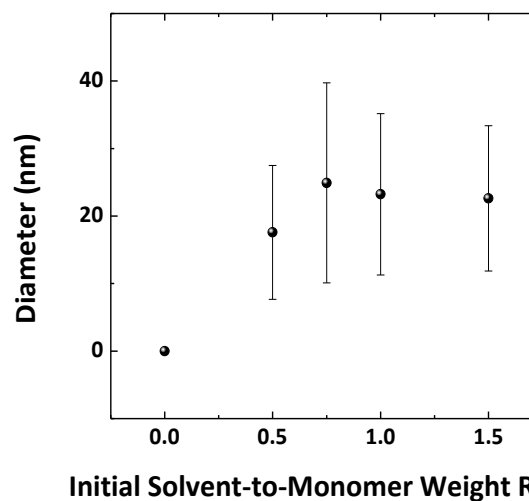


Figure 13. Average pore diameter on the fractured surface vs. initial solvent-to-monomer weight ratio.

The question arises as to whether the observed voids were present before failure. The following discussion serves to answer this question. The surface area fraction occupied by voids was obtained from the images of modified and unmodified systems. These data are reported in Figure 14. For the modified samples broken at ambient temperature void area fractions were not substantially different ranging between 0.5 and 1.2%. If it is assumed that these voids were present before mechanical testing, the area void fractions to calculate density values using the equation below,

$$\rho_2 = (1 - \alpha) * \rho_1 \quad (3)$$

where ρ_2 is predicted density, ρ_1 is the unmodified epoxy density, and α is void-covered area fraction which was measured through image processing of the micrographs. For instance, 1.5 DEA was found to have an average α value of 1.05% from fracture surface micrographs. This yields a predicted density of approximately 1.114 g/cm³. This value is significantly below the average density of the material prior

to tensile deformation. Thus this supports the hypothesis that voids are not pre-existent but a result of protovoid opening and deformation during fracture.

In order to further test this hypothesis, 1.5 solvent-to-monomer weight ratio samples were fractured at liquid nitrogen temperature. This time very few voids were observed using SEM as shown in Figure 15 in which images of cold-fracture and RT-fracture surface morphology for two identical samples are presented. The quantitative measurement of void surface coverage is given in Figure 14 (1.5 DEA-FF) and strongly supports that freeze fractured morphology of the 1.5 DEA sample resembles the RT fracture surface morphology of 0 DEA samples and not that of the 1.5 DEA RT fracture surface (as shown by arrows in Figure 14). The reduced number of visible voids in cold-fracture surface could be due to the speed of crack propagation in cold environments. Experimental studies showed that for viscoelastic materials, a crack propagates faster in a colder environment leading to a reduced value of critical stress intensity factor (K_{Ic}).^{7, 44} Therefore, in colder fracture, the protovoids do not have sufficient time to expand in response to tensile deformation, so fewer holes will be observed on cold-fracture surface micrographs. These results support the conclusion that the observed pores are a result of the fracture event.

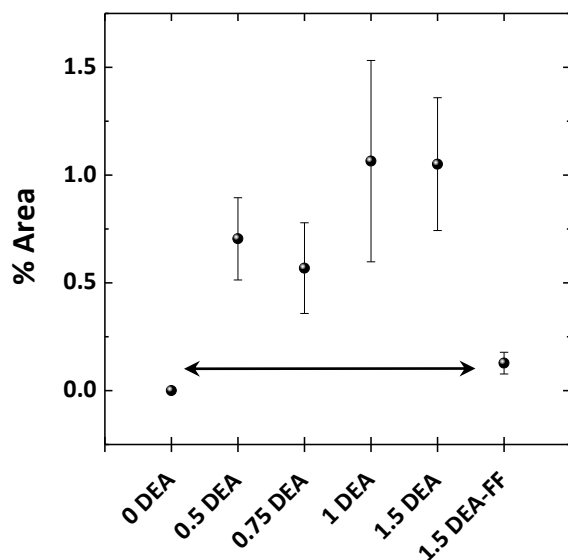


Figure 14. Average surface area covered by voids for RT-fracture surfaces (0 DEA, 0.5 DEA, 0.75 DEA, 1 DEA and 1.5 DEA) and freeze-fracture surfaces (1.5 DEA-FF).

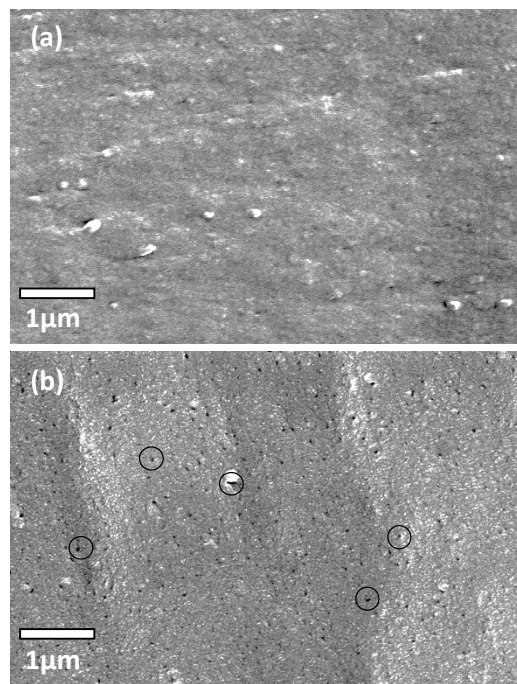


Figure 15. Surface morphology of the modified sample, 1.5 DEA. Freeze-fracture (a) and RT-fracture surface (b). Scale bars are both 1 μm lengthwise. Some of the holes are pointed with circles in the modified (b) structures.

Compressive Properties. The use of data from compression testing is sometimes preferred because phenomena such as crazing and necking are suppressed.⁴⁵ Therefore, to better understand the effect of the protovoids on compressive behaviour of the modified thermosets, the response of those materials to uniaxial compressive load was investigated. In this case true stress-strain values were utilized instead of the engineering convention, since the dimensions of the samples greatly vary during the test. True stress-strain values were evaluated from the engineering stress-strain based on the following equations:⁴⁶

$$\sigma_t = \sigma_e(1 + \varepsilon_e) = \sigma_e \lambda \quad (4)$$

$$\varepsilon_t = \ln(1 + \varepsilon_e) = \ln \lambda \quad (5)$$

Here, λ is the extension ratio which is defined by $\lambda = L/L_0$, σ_t and ε_t are the true stress and true strain, respectively, and σ_e and ε_e are the corresponding engineering values. True stress vs. $(1-\lambda)$ for a typical unmodified sample, 0 DEA, and a modified, 1.5 DEA, are shown in Figure 16.

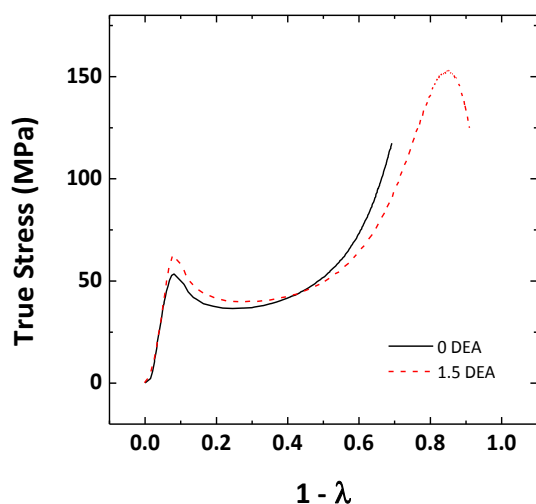


Figure 16. True stress vs. $(1-\lambda)$ for unmodified, 0 DEA, (solid black line) and modified, 1.5 DEA, (red dashed line) in compressive mode.

Values of compressive modulus (E), yield strength (σ_y), and compressive strength (σ_r) based on true stress and strain are listed in Table 4. Results show no significant statistical differences of compressive moduli, compressive strength and compressive yield strength as a function of sample type. This suggests that induced protovoids do not sacrifice the load bearing capacity of the network structures. Also shown in Table 4 are the engineering failure strain (ϵ_r) and plastic deformation ($\epsilon_r - \epsilon_y$) for the series of samples showing that unmodified systems possess significantly lower failure strain and plastic deformation capacity. Thus the modified systems absorb significantly more energy before failure in a manner consistent with the observations obtained from tensile experiments.

Table 4. Compressive properties of 0, 0.5, 0.75, 1 and 1.5 DEA samples.

	E (GPa)	σ_y (MPa)	σ_r (MPa)	ϵ_r (%)	$\epsilon_r - \epsilon_y$ (%)
0 DEA	1.6 ± 0.1	48.7 ± 3.8	138.9 ± 13.1	70.3 ± 2.1	62.9 ± 1.4
0.5 DEA	1.6 ± 0.2	48.9 ± 5.3	141.9 ± 20.1	79.4 ± 3.5	70.3 ± 3.5
0.75 DEA	2.0 ± 0.3	58.6 ± 4.9	185.5 ± 51.1	84.4 ± 3.7	76.4 ± 1.5
1 DEA	1.7 ± 0.2	46.4 ± 6.0	160.7 ± 25.0	85.4 ± 3.4	77.1 ± 2.4
1.5 DEA	2.1 ± 0.2	54.5 ± 6.7	175.0 ± 80.2	86.2 ± 5.4	79.7 ± 4.3

Conclusions

More ductile crosslinked thermosets are obtained by applying a novel processing technique termed reactive encapsulation of solvent/drying, or RESD. SEM images from the fracture surfaces showed clear voids on the modified samples whereas prior to tension, all modified samples had the same density, T_g , Young's modulus of the unmodified epoxy. Modified samples also had the same ultimate tensile strength but much higher ductility compared to the unmodified epoxy. It was shown using all-atom simulations that during-cure solvent species alter the polymer network topology. The presence of distinct topological features in the modified network is likely the origin of the large improvement in ductility. Topology-based toughening is potentially an important step toward developing

better high performance network polymers and composites. Unlike other toughening methods, critical mechanical and thermal properties such as Young's modulus, ultimate tensile strength and glass transition temperature are not sacrificed.

Acknowledgments

The authors acknowledge the financial support from the cooperative agreement between the Materials in Extreme Dynamic Environments (MEDE) Consortium and U.S. Army Research Lab contract W911NF-12-2-0022 as well as support from U.S. Army Research Laboratory under the Army Materials Center of Excellence Program, contract W911NF-06-2-0013. We thank Huntsman Corporation for generous donation of polyetheramine reagents and also Mr. Ian McAninch for his assistance and helpful discussions.

Notes and references

^a Department of Chemical and Biological Engineering, Drexel University, Philadelphia, Pennsylvania 19104, USA.

1. D. R. Askeland and Editor, *The Science and Engineering of Materials, Third Edition*, Chapman & Hall, 1996.
2. S. Ahmad, S. M. Ashraf and A. Hasnat, *Painindia*, 2002, 52, 47-48,50-52.
3. R. Bagheri, B. T. Marouf and R. A. Pearson, *Polym. Rev. (Philadelphia, PA, U. S.)*, 2009, 49, 201-225.
4. R. A. Pearson and A. F. Yee, *Journal of Materials Science*, 1991, 26, 3828-3844.
5. J. D. LeMay and F. N. Kelley, *Adv. Polym. Sci.*, 1986, 78, 115-148.
6. E. M. Petrie, *Epoxy Adhesive Formulations*, McGraw-Hill, 2006.
7. A. Kinloch, Springer Berlin / Heidelberg, 1985, vol. 72, pp. 45-67.
8. D. Mukherji and C. F. Abrams, *Physical Review E*, 2008, 78, 050801.
9. D. Mukherji and C. F. Abrams, *Physical Review E*, 2009, 79, 061802.
10. R. D. Brooker, A. J. Kinloch and A. C. Taylor, *The Journal of Adhesion*, 2010, 86, 726-741.
11. A. J. Kinloch, M. L. Yuen and S. D. Jenkins, *J. Mater. Sci.*, 1994, 29, 3781-3790.
12. K. Dusek, F. Lednický, S. Lunak, M. Mach and D. Duskova, *Adv. Chem. Ser.*, 1984, 208, 27-35.
13. E. H. Rowe, A. R. Siebert and R. S. Drake, *Mod. Plast.*, 1970, 47, 110-112, 114, 116-117.
14. R. Bagheri and R. A. Pearson, *J. Mater. Sci.*, 1996, 31, 3945-3954.
15. J. Choi, A. F. Yee and R. M. Laine, *Macromolecules*, 2004, 37, 3267-3276.
16. A. F. Yee and R. A. Pearson, *Journal of Materials Science*, 1986, 21, 2462-2474.
17. J. M. Dean, N. E. Verghese, H. Q. Pham and F. S. Bates, *Macromolecules*, 2003, 36, 9267-9270.
18. Z. J. Thompson, M. A. Hillmyer, J. Liu, H.-J. Sue, M. Dettloff and F. S. Bates, *Macromolecules*, 2009, 42, 2333-2335.
19. Y. S. Thio, J. Wu and F. S. Bates, *Macromolecules*, 2006, 39, 7187-7189.
20. H. Harani, S. Fellahi and M. Bakar, *Journal of applied polymer science*, 1999, 71, 29-38.
21. V. I. Raman and G. R. Palmese, *Colloids Surf., A*, 2004, 241, 119-125.
22. V. I. Raman and G. R. Palmese, *Langmuir*, 2005, 21, 1539-1546.

23. S. Karad and F. Jones, presented in part at the Composites Technologies for 2020: , University of Sydney, Australia, 2004.
24. M. B. Robertson, I. M. Ward, P. G. Klein and K. J. Packer, *Macromolecules*, 1997, 30, 6893-6898.
25. D. F. Rohr and M. T. Klein, *Ind. Eng. Chem. Res.*, 1988, 27, 1361-1366.
26. D. F. Rohr and M. T. Klein, *Ind. Eng. Chem. Res.*, 1990, 29, 1210-1218.
27. G. R. Palmese and R. L. McCullough, *J. Appl. Polym. Sci.*, 1992, 46, 1863-1873.
28. V. I. Raman and G. R. Palmese, *Macromolecules*, 2005, 38, 6923-6930.
29. D. R. Lide, *CRC handbook of chemistry and physics*, CRC press, 2012.
30. J. Mijovic and S. Andjelic, *Macromolecules*, 1995, 28, 2787-2796.
31. J. Wang, W. Wang, P. A. Kollman and D. A. Case, *J. Mol. Graphics Modell.*, 2006, 25, 247-260.
32. J. Wang, R. M. Wolf, J. W. Caldwell, P. A. Kollman and D. A. Case, *J. Comput. Chem.*, 2004, 25, 1157-1174.
33. S. Plimpton, *J. Comput. Phys.*, 1995, 117, 1-19.
34. K. S. Khare and R. Khare, *Macromol. Theory Simul.*, 2012, 21, 322-327.
35. E. W. Dijkstra, *Numerische mathematik*, 1959, 1, 269-271.
36. C. Jang, M. Sharifi, C. F. Abrams and G. R. Palmese, *Polymer*, 2014.
37. M. J. Marks, N. E. Verghese, K. J. Hrovat, A. Laboy-Bollinger, J. C. Buck, J. A. Rabon, Jr., C. L. O'Connell and L. Allen, *J. Polym. Sci., Part B: Polym. Phys.*, 2008, 46, 1632-1640.
38. L. E. Nielsen, *Mechanical Properties of Polymers and Composites, Vol. 1*, Dekker, 1974.
39. J. Mark, *Chem. Ind. (London, U. K.)*, 2007, 29-30.
40. C. W. Macosko and D. R. Miller, *Macromolecules*, 1976, 9, 199-206.
41. A. T. DiBenedetto, *J. Polym. Sci., Part B: Polym. Phys.*, 1987, 25, 1949-1969.
42. L. E. Nielsen, *J. Macromol. Sci., Rev. Macromol. Chem.*, 1969, 3, 69-103.
43. J. P. Pascault and R. J. J. Williams, *Polym. Bull. (Berlin)*, 1990, 24, 115-121.
44. T. L. Anderson and Editor, *Fracture Mechanics: Fundamentals and Applications; Third Edition*, CRC Press, 2005.
45. H. G. H. van Melick, L. E. Govaert and H. E. H. Meijer, *Polymer*, 2003, 44, 3579-3591.
46. D. Roylance, *Massachusetts Institute of Technology study, Cambridge*, 2001.

PAPER

ToC description:

A new toughening mechanism for thermosetting polymers is shown. The technique involves manipulation of polymer network topology allowing the glassy material to deform under loading without rupturing covalent bonds.

